The Astrophysical Journal Letters, 958:L40 (13pp), 2023 December 1 https://doi.org/10.3847/2041-8213/ad0bd9

Accretion-modified Stars in Accretion Disks of Active Galactic Nuclei: The Low-luminosity Cases and an Application to Sgr A*

Jian-Min Wang[1,2,3], Jun-Rong Liu[1,4], Yan-Rong Li[1], Yu-Yang Songsheng[1], Ye-Fei Yuan[5], and Luis C. Ho[6,7]
[1] Key Laboratory for Particle Astrophysics, Institute of High Energy Physics, Chinese Academy of Sciences, 19B Yuquan Road, Beijing 100049, People's Republic of China
[2] School of Astronomy and Space Sciences, University of Chinese Academy of Sciences, 19A Yuquan Road, Beijing 100049, People's Republic of China
[3] National Astronomical Observatory of China, 20A Datun Road, Beijing 100020, People's Republic of China
[4] School of Physics, University of Chinese Academy of Sciences, 19A Yuquan Road, Beijing 100049, People's Republic of China
[5] Department of Astronomy, University of Science and Technology of China, Hefei 230026, Anhui, People's Republic of China
[6] Kavli Institute of Astronomy and Astrophysics, Peking University, Beijing 100871, People's Republic of China
[7] Department of Astronomy, Peking University, Beijing 100871, People's Republic of China
Received 2023 August 23; revised 2023 November 8; accepted 2023 November 10; published 2023 December 6

Abstract

In this paper, we investigate the astrophysical processes of stellar-mass black holes (sMBHs) embedded in advection-dominated accretion flows (ADAFs) of supermassive black holes (SMBHs) in low-luminosity active galactic nuclei. The sMBH is undergoing Bondi accretion at a rate lower than the SMBH. Outflows from the sMBH-ADAF dynamically interact with their surroundings and form a cavity inside the SMBH-ADAF, thereby quenching the accretion onto the sMBH. Rejuvenation of the Bondi accretion is rapidly done by turbulence. These processes give rise to quasi-periodic episodes of sMBH activities and create flickerings from relativistic jets developed by the Blandford–Znajek mechanism if the sMBH is maximally rotating. Accumulating successive sMBH-outflows trigger a viscous instability of the SMBH-ADAF, leading to a flare following a series of flickerings. Recently, the similarity of near-infrared flare's orbits has been found by GRAVITY/VLTI astrometric observations of Sgr A*: their loci during the last 4 yr consist of a ring in agreement with the well-determined SMBH mass. We apply the present model to Sgr A*, which shows quasi-periodic flickerings. An sMBH of $\sim 40 M_{\odot}$ is preferred orbiting around the central SMBH of Sgr A* from fitting radio to X-ray continuum. Such an extreme mass ratio inspiraling provides an excellent laboratory for LISA/Taiji/Tianqin detection of mHz gravitational waves with strains of $\sim 10^{-17}$, as well as their polarization.

Unified Astronomy Thesaurus concepts: Active galaxies (17)

1. Introduction

The model of accretion onto a single supermassive black hole (SMBH) is successful to explain the powerful radiation of active galactic nuclei (AGNs; e.g., Rees 1984); however, there is a growing body of evidence suggesting that some new ingredients should be incorporated into this canonical model. Star formation has been suggested by many authors for different purposes since the early attempts of Kolykhalov & Sunyaev (1980) in light of the self-gravity of outer parts of the AGN accretion disks (Paczyński 1978). Consequently, it may be an efficient way of fueling gas to galactic centers, triggering the activity of SMBHs (Shlosman & Begelman 1989; Thompson et al. 2005; Wang et al. 2010). Spectral energy distributions (SEDs) of AGNs could be revised by star formation (Goodman 2003; Goodman & Tan 2004; Thompson et al. 2005) as well as the origins of high metallicity (Collin & Zahn 1999, 2008; Wang et al. 2011, 2012b, 2023; Grishin et al. 2021; Fan & Wu 2023) observed in AGN broad-line regions (Hamann & Ferland 1999; Warner et al. 2003; Nagao et al. 2006; Shin et al. 2013; Du & Wang 2014). After supernovae explosions of stars formed in the AGN disks, there remain compact objects as satellites of the central SMBHs. Obvious questions remain as to the fates of the satellites embedded in the disks, what is their observational appearance?

The potential association of quasar SDSS J1249 + 3449 with GW190521 (Graham et al. 2020), consisting of $(85 + 66) M_{\odot}$ binary BHs, by the Advanced LIGO/Virgo consortium (Abbott et al. 2020) was motivated by the formation of such a massive BH binary in special environments. See more candidates of potential associations of LIGO gravitational wave (GW) detection with quasars (Graham et al. 2023). These mergers of high-mass stellar black hole (BH) binaries are much beyond productions from the evolution of stars (Woosley et al. 2002), indicating that they are formed in a very dense environment. They have stimulated renewed interest in the question of the fates of compact objects in the AGN disks (e.g., McKernan et al. 2012; Bellovary et al. 2016; Bartos et al. 2017; Stone et al. 2017; Secunda et al. 2019; Yang et al. 2019; Graham et al. 2020; Tagawa et al. 2020; Wang et al. 2021a, 2021b; Samsing et al. 2022). This interesting idea can be traced back to the early paper of Cheng & Wang (1999), who suggest that compact objects formed in AGN disks undergo mergers generating γ-ray bursts and GWs. The terminology of accretion-modified stars (AMS) used in this series are referred to as ones with accretion from AGN disks (Wang et al. 2021a), where the accreting objects could be main-sequence stars (Wang et al. 2023), stellar-mass BHs (sMBHs; Wang et al. 2021b), neutron stars (Zhu et al. 2021b), or white dwarf stars (Zhu et al. 2021a; Zhang et al. 2023). AMS phenomena exhibit distinguished features in different environments as predicted by the above papers.

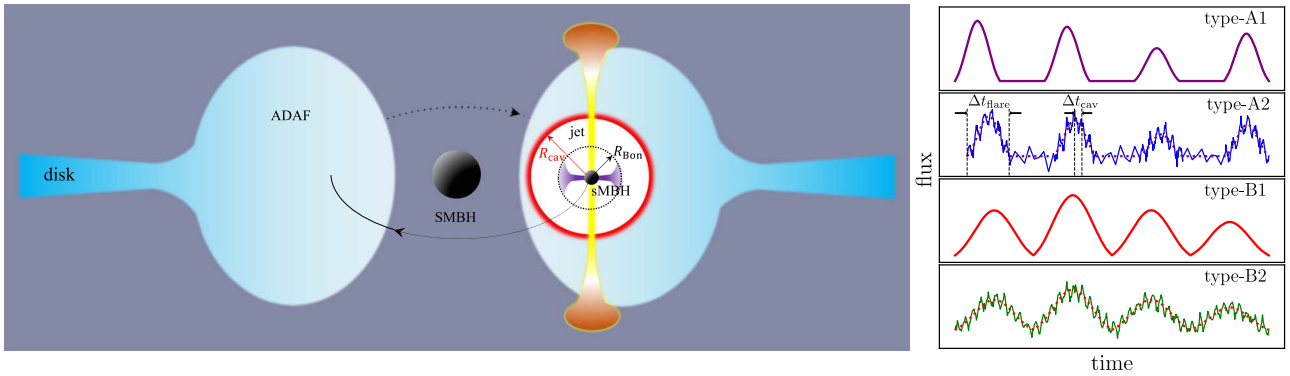

Figure 1. Left: an sMBH embedded in SMBH-ADAFs is orbiting around the central SMBH. The sMBH is accreting with Bondi rates from the SMBH-ADAF, but outflows from the sMBH-ADAFs drive the formation of a cavity and quench the accretion. Such an accretion-feedback system exhibits quasi-periodic behaviors, showing quasi-periodic flickerings from relativistic jets produced through the Blandford–Znajek (BZ) mechanism of the sMBH-ADAF. Emissions of the jet constitute spectral energy distributions additional to the SMBH-ADAF. The jet may be partially choked by the SMBH-ADAF, giving rise to subrelativistic wisps from the SMBH-ADAF. The accumulating sMBH-outflows will trigger the viscosity instability of the SMBH-ADAF resulting in flares following a series of flickerings. The present model can explain the NIR quasi-periodic flickerings and flares of Sgr A*. Right: illustrated classifications of light curves. Type-A shows that flares and/or flickerings are superposed on a stationary state whereas type-B shows an upon-down mode. Flickerings are thin lines, and flares are thick lines.

This is the third paper of the series exploring the observational signatures of accreting BHs in contexts of AGN accretion disks (Wang et al. 2021a, 2021b). The sMBHs have been studied in the environment of standard accretion disks (Wang et al. 2021a) showing electromagnetic signatures of the Bondi explosion, and Jacobi capture (sMBHs are captured by each other through their tidal forces in nearby orbits around the central SMBHs; Wang et al. 2021b). This paper focuses on studying the signatures of sMBH embedded in advection-dominated accretion flows (ADAFs) of low-luminosity AGNs (LLAGNs). Quasi-periodic flickerings are suggested to occur over the whole electromagnetic wave bands. Flares following a series of flickerings are produced by accumulated energies of the sMBH-outflows. We apply the present model to Sagittarius A* (Sgr A*) for its variabilities and multiwavelength emissions in Section 3. Sgr A* is an excellent laboratory of milli-Hertz (mHz) GWs.

2. The Model

Figure 1 shows the model of the present AMS. An sMBH (the secondary BH as one satellite of the SMBH) is orbiting around the central SMBH (the primary) inside the ADAF. We assume a circular orbit in this binary BH system. Parameters with the subscripts of "s" and "p" are referred to as those of the secondary and the primary. Their dimensionless accretion rates are defined by $\dot{\mathscr{M}}_{\rm p,s}=\dot{M}_{\rm p,s}/\dot{M}^{\rm p,s}_{\rm Edd}$, where $\dot{M}_{\rm p,s}$ are the accretion rates, $\dot{M}^{\rm p,s}_{\rm Edd}=L^{\rm p,s}_{\rm Edd}c^{-2}$ is their corresponding limit rate in light of the Eddington luminosity $L^{\rm p,s}_{\rm Edd}=4\pi GM_{\rm p,s}m_{\rm p}c/\sigma_{\rm T}$, where G is the gravitational constant, c is the speed of light, $m_{\rm p}$ is the proton mass, and $\sigma_{\rm T}$ is the Thomson cross section. When $\dot{M}$ is much less than the unity, the accretion flows are supported by the ion pressure of the plasma with two temperatures because cooling is so inefficient that most of the released energies are not able to radiate away. This results in the accretion flows being very hot and able to produce relativistic jet (Rees et al. 1982). This is the early version of ADAF. For simplicity, we use the self-similar solution of ADAF for the primary BH (Narayan & Yi 1995), in which the half-thickness, density, and sound velocity are

$$\begin{cases} H_{\rm p} &= 1.2\times10^{12}\,M_6 r_1\ {\rm cm},\\ n_{\rm e} &= 9.3\times10^{9}\,\alpha_{0.1}^{-1}M_6^{-1}\dot{\mathscr{M}}_{\rm p,\bar{3}}r_1^{-3/2}\ {\rm cm^{-3}},\\ c_{\rm s,p} &= 5.0\times10^{9}\,r_1^{-1/2}\ {\rm cm\ s^{-1}},\\ v_{\rm r} &= 3.9\times10^{8}\,\alpha_{0.1}r_1^{-1/2}\ {\rm cm\ s^{-1}}, \end{cases} \quad (1)$$

where $\alpha_{0.1}=\alpha/0.1$ is the viscosity parameter (Shakura & Sunyaev 1973), $r_1=R_{\rm .}/10R_{\rm g}$ is the radius of the disk from the SMBH, and $R_{\rm g}=GM_{\rm p}/c^2$ is the gravitational radius, $\dot{\mathscr{M}}_{\rm p,\bar{3}}=\dot{\mathscr{M}}_{\rm p}/10^{-3}$, and $M_6=M_{\rm p}/10^6M_\odot$ is the mass of the primary BH. There are three constants of $c_{1,2,3}$ in the self-similar solution (Narayan & Yi 1995). In the case of an advection fraction ($f_{\rm adv}=0.9$, and the adiabatic index of $\gamma=4/3$), we calculate the three constants of $c_{1,2,3}=(0.42, 0.55, 0.28)$ from their definitions in this paper. Although the self-similar solution is used here, it is in agreement with the numerical solutions of the global ADAF. The density given by Equation (1) is consistent with Chandra X-ray observations of Sgr A*, where the column density $N_{\rm H}\approx8.0\times10^{22}\,{\rm cm^{-2}}$ at the center (Wang et al. 2013), which is consistent with the inward extrapolation of the gas density from the Bondi radius (Xu et al. 2006). The ADAF scattering optical depth is about $\tau_{\rm es}\approx0.007$ at $10\,R_{\rm g}$ in the vertical direction for these typical values given by Equation (1), leading to different situations from the Shakura–Sunyaev disks; the jet developed by the sMBH could be not completely choked. The most prominent feature of the ADAF is the positive Bernoulli constant (defined as a sum of kinematic, thermal, and potential energies of the ADAF gas), implying that outflows are developed by the advection mechanism since the accretion flows become gravitationally unbound by the SMBH (Narayan & Yi 1994). Although the radiative efficiency of the ADAF is very low, the efficiency of outflows is quite high, resulting in strong feedback to the SMBH-ADAF and making a cavity around the sMBH.

For simplicity, we assume that the sMBH is trapped inside the SMBH-ADAF, and its Bondi accretion rates are given by

$$\dot{\mathscr{M}}_{\rm s}=\frac{\dot{M}_{\rm s}}{\dot{M}_{\rm Edd}}=\frac{4\pi G^2M_{\rm s}^2\rho_{\rm p}}{c_s^3\dot{M}_{\rm Edd}}=2.0\times10^{-6}\,\alpha_{0.1}^{-1}\dot{\mathscr{M}}_{\rm p,\bar{3}}q_{\bar{5}}, \quad (2)$$

where $M_{\rm s}$ is the mass of sMBH, $q_{\bar{5}}=q/10^{-5}$, $q=M_{\rm s}/M_{\rm p}$ is the mass ratio of the sMBH to the central SMBH, and $\rho_{\rm p}=n_em_{\rm p}$ is the mass density of the SMBH-ADAF. This indicates that the sMBH is also the status of ADAF. It is interesting to note that the sMBH accretion rates are independent of its location. The Bondi radius of the sMBH

$$R_{\rm Bon}=\frac{GM_{\rm s}}{c_{\rm s,p}^2}=2.1\times10^8\left(\frac{m_1}{4}\right)r_1\,{\rm cm}, \quad (3)$$

where $m_1=M_{\rm s}/10\,M_\odot$ is the sMBH mass. $R_{\rm Bon}$ is much smaller than the Hill radius of $R_{\rm Hill}=(M_{\rm s}/M_{\rm p})^{1/3}R_{\bullet}\approx 3.2\times10^{10}\,m_1^{1/3}M_6^{2/3}r_1$ cm; the SMBH tidal disruption of the AMS can be avoided. On the other hand, the outer radius (or the circularized radius) of the sMBH-ADAF can be estimated by angular momentum (AM) balance. The net specific AM of the SMBH-ADAF is given by $\Delta\ell_{\rm p}=\Delta R\sqrt{GM_{\rm p}/R_{\bullet}}$, where ΔR is the width of the belt at R. The specific AM of the sMBH-ADAF can be approximated by $\Delta\ell_{\rm s}=\sqrt{X_{\rm out}GM_{\rm s}}$, where $X_{\rm out}$ is the outer radius of the sMBH-ADAF. Equating $\Delta\ell_{\rm p}=\Delta\ell_{\rm s}$ and $\Delta R\approx X_{\rm out}$, we have approximately $X_{\rm out}=(M_{\rm s}/M_{\rm p})R_{\bullet}=1.5\times10^7\,q_{\bar{5}}r_1M_6$ cm, which is consistent with numerical simulations (e.g., Igumenshchev et al. 1999). The $X_{\rm out}$ is significantly smaller than the Bondi radius.

It should be noted that the orbiting sMBH suggested here is rotating with a supersonic velocity ($v_{\rm rot}\sim c/3$) at $10\,R_{\rm g}$. Shocks due to the motion could be produced to accelerate some electrons. Subsequently, nonthermal emissions of the electrons are thus radiated from this region. A similar case of the Bondi sphere of an isolated BH supersonically moving in medium has been discussed by Wang & Loeb (2014); however, we will not discuss this potentially important point here. In this paper, only the case with an extremely low-q system is considered. Such a system allows us to use the perturbation approximation to treat the influence of the sMBH on the SMBH-ADAF. Otherwise, we have to consider the inhomogeneity of the SMBH-ADAF caused by the sMBH feedback. We consider that the SMBH-ADAF is in a stationary state.

2.1. Cavity and Flares

Since the progenitor of the sMBH should rotate very fast, the sMBH should also rotate fast and undergo two processes to generate influence on the SMBH-ADAF. First, energetic outflows with a power of $L_{\rm out}=\eta_{\rm out}\dot{M}_{\rm s}c^2$ are produced since the Bernoulli constant is positive, where $\eta_{\rm out}$ is the conversion efficiency of channeling gravitational energy into outflows. We note that $\eta_{\rm out}$ is much higher than the radiative efficiency of the ADAF and take $\eta_{\rm out}=0.1$ as a typical value in this paper. The higher $\eta_{\rm out}$, the more prominent effects of the sMBH on the SMBH-ADAF. Second, the Blandford–Znajek processes (BZ: Blandford & Znajek 1977) form bipolar relativistic jets. The outflows from sMBH-ADAF heat gas within the Bondi radius are efficiently clearing the gas in a timescale of $\Delta t_{\rm Bon}=\Delta E_{\rm Bon}/L_{\rm out}$, where $\Delta E_{\rm Bon}=GM_{\rm s}\Delta M_{\rm Bon}/R_{\rm Bon}$ is the gravitational energy of the gas, and $\Delta M_{\rm Bon}\approx\frac{4\pi}{3}R_{\rm Bon}^3n_em_{\rm p}$ is the gas mass within $R_{\rm Bon}$. For $n_e=10^{10}\,{\rm cm}^{-3}$, we have $t_{\rm Bon}\sim0.017$ s, and this demonstrates the sMBH-outflows have efficient feedback to form a cavity in the SMBH-ADAF. On the other hand, the smearing timescale of the Bondi cavity is approximately $R_{\rm Bon}/\alpha c_{\rm s}\sim10^{-3}$ s. In the Appendix, we list the other two classes of cavity formation. They have timescales much longer than $t_{\rm Bon}$, but significantly shorter than the flickerings and flares in Sgr A*. Moreover, the cooling timescale of local SMBH-ADAF is much longer than these cases. It can be regarded as a successive series of these events that create a cavity as described below.

Outflows from the sMBH-ADAF will significantly affect the local structures of the SMBH-ADAF, generating a cavity with a radius of $R_{\rm cav}$, provided that the outflow kinetic energies exceed the local dissipation rates of gravitational energy of the SMBH-ADAF. This condition can be expressed as

$$L_{\rm out}\gtrsim\frac{4\pi}{3}R_{\rm cav}^3\varepsilon_+, \quad (4)$$

where $\varepsilon_+\approx Q_+/H_{\rm p}$ is the volume dissipation rates of the SMBH-ADAF; $Q_+=3GM_{\rm p}\dot{M}_{\rm p}/8\pi R_{\bullet}^3$ is surface rates (Frank et al. 2002). Here, we neglect the factor of the inner boundary condition of accretion disks. We would like to point out the implications of Equation (4), i.e., the outflow energies are the extra source of the SMBH-ADAF as type-A variability shown in Figure 1. In the following discussions, we take the equal form of inequality (4), and some results are the upper and lower limits for a given $L_{\rm out}$, for instance, $R_{\rm cav}$ in Equation (6) and $\Delta t_{\rm cav}$ in Equation (7), respectively. The cavity can be made by the work done within a time interval $\Delta t_{\rm cav}$ through the outflow-driven expansion of the heated part

$$L_{\rm out}\Delta t_{\rm cav}=\frac{4\pi}{3}R_{\rm cav}^3P_{\rm gas}, \quad (5)$$

where $P_{\rm gas}=\rho_{\rm p}c_{\rm s}^2$ is the gas pressure of the SMBH-ADAF. Actually, Equation (5) shares the same meaning of the work done as $P\Delta V$ of AGN feedback in galaxy cluster (e.g., McNamara & Nulsen 2007; Fabian 2012). The ram pressure of the sMBH-outflows impedes the inflows outside the cavity through the balance with the surrounding medium, namely $L_{\rm out}/v_{\rm out}=4\pi R_{\rm cav}^2P_{\rm gas}$. We find that this condition holds as long as the outflows have a Mach number of $\mathcal{M}=v_{\rm out}/c_{\rm s}\geqslant1$. Equation (5) describes the working process of cavity formation, and is independent of Equation (4). In the Appendix, we discuss the other two possibilities of cavity formation and find that they naturally satisfy the conditions (Equations (4) and (5)) employed here. During the cavity formation, we approximate the gas pressure as a constant. From this energy budget, we can derive the cavity radius

$$\begin{aligned}R_{\rm cav}&=\left(\frac{3L_{\rm out}H}{4\pi Q_+}\right)^{1/3}\\&=1.9\times10^{10}\eta_{0.1}^{1/3}\alpha_{0.1}^{-1/3}r_1^{4/3}q_{\bar{5}}^{2/3}\left(\frac{M_6}{4}\right){\rm cm}, \quad (6)\end{aligned}$$

and the time for cavity formation

$$\Delta t_{\rm cav}=\frac{HP_{\rm gas}}{Q_+}=45.9\,\alpha_{0.1}^{-1}r_1^{3/2}\left(\frac{M_6}{4}\right)\,{\rm minutes}, \quad (7)$$

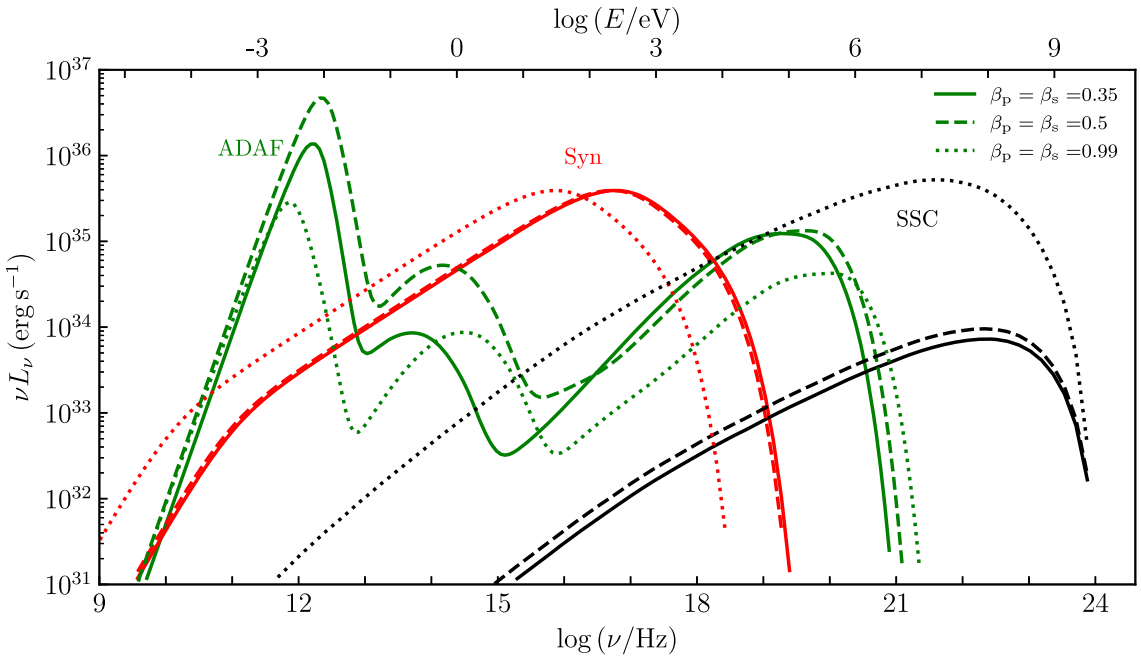

Figure 2. The overall spectral energy distributions of the SMBH-ADAF and the relativistic jets from the sMBH. The relativistic jet mainly contributes to the optical to soft X-ray bands. In these calculations, we take the same values of the magnetization parameter ($\beta_{p,s}$) in the SMBH- and sMBH-ADAFs. See text for values of model parameters.

where $\eta_{0.1} = \eta_{\rm out}/0.1$. $R_{\rm cav}$ is comparable to the Hill radius, but is still much smaller than the half-thickness of the SMBH-ADAF. In the case of the SMBH-ADAF, $R_{\rm cav}$ is independent of the accretion rates of the SMBH-ADAF, but dependent of the location and mass of the sMBH, and the SMBH mass. Since $R_{\rm cav} \gg R_{\rm Bon}$, the sMBH will stop accretion in the timescale of the cavity formation. It is very interesting to note that the formation timescale is independent of the sMBH and its outflows but sensitive to its location radius and the SMBH mass. This offers an opportunity to measure the viscosity as the hardest parameter of accretion macro-physics if the location, sMBH mass, and flickering periods are fixed in the future (after detections of mHz GWs). Actually, this $\Delta t_{\rm cav}$ is just the thermal instability timescale of $t_{\rm therm} = \Sigma c_{\rm s}^2/Q_+$ (e.g., Frank et al. 2002). We get this from the energy budget avoiding details of the expansion dynamics. Simultaneously, we should note that the BZ process generates relativistic ejecta during $\Delta t_{\rm cav}$. This produces flickerings as a result of the quenched Bondi accretion of the sMBH-outflows.

On the other hand, this cavity could be slacked down by the dynamical interaction or turbulence after the cessation of outflows. This rejuvenates the Bondi accretion of the sMBH. For a simple estimation, we can estimate the timescale of a rejuvenation

$$\Delta t_{\rm rej} = \frac{R_{\rm cav}}{v_{\rm tur}} = 37.9\, \eta_{0.1}^{1/3} \alpha_{0.1}^{-4/3} q_5^{2/3} r_1^{11/6} \left(\frac{M_6}{4}\right) {\rm s}, \qquad (8)$$

where $v_{\rm tur} = \alpha c_{\rm s}$ is the turbulence velocity, which is much shorter than $\Delta t_{\rm cav}$. The cavity is then destroyed by the turbulence of the cavity developed by the interaction between the outflows and the SMBH-ADAF. It is therefore expected that the cavity appears periodically with a timescale of $\Delta t_{\rm cav} + \Delta t_{\rm rej} \approx \Delta t_{\rm cav}$. A flickering lasts for $\Delta t_{\rm cav}$. It is very interesting to note that $\Delta t_{\rm cav}$ only sensitively depends on the location of the sMBH given the binary masses. From the observational side, the flickering period can be used to estimate the location. In practice, if the density of the SMBH-ADAF could be inhomogeneous, the flickering timescale could vary at different epochs. On the averaged behaviors, the sMBH undergoes quasi-periodic activities appearing as quasi-periodic flickerings. This is a unique feature of the AMS inside SMBH-ADAFs.

The sMBH is undergoing episodic Bondi accretion, but the cavity continually grows with time since the SMBH-ADAF is cooling much slower than the outflow-driven heating of the sMBH-ADAF. Therefore, the cavity density decreases, but its temperature and radius increase with time. Cooling processes inside the SMBH-ADAF involve bremsstrahlung (proton–electron and electron–electron collisions), synchrotron radiation, and inverse Compton (IC) scattering (e.g., Narayan & Yi 1995). Magnetic fields are usually estimated by the magnetization factor β, which is defined by $P_{\rm gas} = \beta(P_{\rm gas} + P_{\rm mag})$, where $P_{\rm mag} = B^2/8\pi$ is the magnetic pressure, and B is magnetic field. For the case of $\beta = 0.5$, $n_e = 10^{10}\,{\rm cm}^{-3}$, and $T_{\rm e} = 10^9$ K, we obtain the total emissivity of $\epsilon_{\rm tot} \approx \chi\, \epsilon_{\rm ff}$, and $\chi \approx 28$ (this can also be justified by comparing the near-IR (NIR) and hard X-ray peaks of ADAF SED as shown in Figure 2), where $\epsilon_{\rm ff}$ is the free–free emissivity. The cooling factor χ depends on the density, temperature, and magnetization factor β. The cooling timescale of the shocked gas

$$\Delta t_{\rm cool} = \frac{3}{2}\frac{n_{\rm e} k T_{\rm s}}{\epsilon_{\rm tot}} \approx 5.6\, \chi_0^{-1} T_9^{1/2} n_{10}^{-1}\, {\rm hr}, \qquad (9)$$

where $\chi_0 = \chi/28$, $n_{10} = n_e/10^{10}\,{\rm cm}^{-3}$, k is the Boltzmann constant, and $T_9 = T_{\rm s}/10^9$ K is the temperature of the shocked SMBH-ADAF. Since $\Delta t_{\rm cool} \gg \Delta t_{\rm cav}$, the SMBH-ADAF gas

will be continuously heated by the sMBH-ADAF outflows, and the cavity grows with time. When it reaches the cooling timescale, the sMBH outflow accumulates power enough to produce a flare with a cavity radius

$$R_{\rm flare} \approx \left(\frac{3L_{\rm out}\Delta t_{\rm cool}}{4\pi P_{\rm gas}}\right)^{1/3} = 3.7\times10^{10}\,\eta_{0.1}^{1/3}\chi_0^{-1/3}T_9^{1/6}n_{10}^{-1/3}r_1^{5/6}q_{\bar{5}}^{2/3}\left(\frac{M_6}{4}\right)^{2/3}\ {\rm cm}, \quad (10)$$

from Equation (5), which is still much smaller than the thickness of the SMBH-ADAF. The viscous instability of the SMBH-ADAF is developing in a timescale of $\Delta t_{\rm vis}\approx\alpha^{-1}(H/R_\bullet)^{-2}t_\phi$, where t_ϕ is the orbit period (e.g., Frank et al. 2002). For typical values and $H/R_\bullet\sim1$, we have $\Delta t_{\rm vis}\approx 11.0\,\alpha_{0.1}^{-1}(M_6/4)r_1^{3/2}$ hr, which is comparable with the cooling timescale. Therefore, the viscous instability will be unavoidably triggered by the accumulated energies of the sMBH-ADAF outflows. A flare releases the total energies of

$$E_{\rm flare}\approx\Delta t_{\rm flare}Q_+(\pi R_{\rm flare}^2) \approx 1.5\times10^{40}\,\eta_{0.1}^{2/3}\chi_0^{-5/3}T_9^{5/6}n_{10}^{-5/3}r_1^{-4/3}\dot{\mathscr{M}}_{\rm p,\bar{3}}q_{\bar{5}}^{4/3}\left(\frac{M_6}{4}\right)^{1/3}{\rm erg}, \quad (11)$$

where $\Delta t_{\rm flare}=\min(\Delta t_{\rm vis},\Delta t_{\rm cool})$, and we take $\Delta t_{\rm flare}=\Delta t_{\rm cool}$ here for a simple treament. A flare is rising with $\Delta t_{\rm flare}$, and decaying with $\Delta t_{\rm cool}$. The present model predicts that flares happen at a timescale of a few hours ($\Delta t_{\rm flare}$), and a few flares per day. However, the quiescent phase ($\Delta t_{\rm quiet}$) is complicated by the recovery of the flaring cavity of the SMBH-ADAF, which is controlled mainly by local cooling, viscosity-driven infalling gas of the local flows, and viscosity dissipations of the gravitational energies. Flares are not periodic because of uncertainties of $\Delta t_{\rm quiet}$. This unique feature can be used to test the flickering origins (e.g., magnetic reconnection model). As we can see, this is in agreement with the observed flares in Sgr A*. For a flare state, the recovery of the SMBH-ADAF returning to its thermal equilibrium depends on joint processes of cooling and dynamical mixing, rather than a single process. Perturbation approximation is not valid in the state.

We would like to emphasize that the current treatments consider the sMBH activity as a perturbation. The validity of this approximation can be guaranteed provided that the expansion velocity of the cavity formation is subrelativistic. When the mass ratio is large enough, the formation of a cavity will be different from the present. In such a case, the tidal torque of the sMBH-SMBH binary system is strong enough to engulf the SMBH-ADAF. This is very similar to the case of exoplanet formation. The accretion rates of the sMBH are much lower than those in Equation (2) since the SMBH-ADAF density should be replaced by the density inside the gulf; however, it still significantly radiates for observations (since sMBH is large).

2.2. Quasi-periodic Flickerings

Except for outflows from the sMBH-ADAF, relativistic ejecta would be developed by the BZ mechanism through extracting spin energy of the sMBH if it is rotating fast enough (Blandford & Znajek 1977). Given a BH with spin AM $\mathcal{J}_\bullet$, the pumping power is given (Macdonald & Thorne 1982; Ghosh & Abramowicz 1997)

$$L_{\rm BZ}=\left(\frac{1}{32}\right)\omega_{\rm F}^2B_\perp^2R_{\rm h}^2c\left(\frac{\mathcal{J}_\bullet}{\mathcal{J}_{\rm max}}\right)^2, \quad (12)$$

where $B_\perp$ is magnetic field B normal to the horizon at $R_{\rm h}$, $\mathcal{J}_{\rm max}$ is the maximum of the spin AM, and $\omega_{\rm F}=\Omega_{\rm F}(\Omega_{\rm h}-\Omega_{\rm F})/\Omega_{\rm h}^2$ is the factor describing relative angular velocity of magnetic field to the BH ($\Omega_{\rm h}$). The large scale magnetic field of the sMBH-ADAF $B_\perp=B_{\rm disk}(H/r_\bullet)^{1/2}$; $r_\bullet$ is the radius of the sMBH disk, which is formed by the fast radial motion (Livio et al. 2003; Cao 2011), and this will be involved to form a jet, where $B_{\rm disk}$ is the azimuthal magnetic fields generated by the dynamo viscosity. Generally, geometrically thin disks ($H/r_\bullet\sim10^{-2}$–10^{-3}) are not able to produce relativistic jets because of $B_\perp\ll B_{\rm disk}$. It should be noted that the sMBH-ADAF has much stronger $B_{\rm disk}$ than that of the SMBH-ADAF, which can be justified by Equation (2.15) in Narayan & Yi (1995). For an optically thin ADAF, Armitage & Natarajan (1999) calculated the BZ power

$$L_{\rm BZ}\approx\frac{\sqrt{14}}{192}j_\bullet^2\dot{M}_{\rm s}c^2 =1.92\times10^{32}\,\alpha_{0.1}^{-1}j_\bullet^2\dot{\mathscr{M}}_{\rm p,\bar{3}}q_{\bar{5}}^2\left(\frac{M_6}{4}\right){\rm erg\ s^{-1}}, \quad (13)$$

where $j_\bullet=\mathcal{J}_\bullet/\mathcal{J}_{\rm max}$, and we use the Bondi accretion rates (Equation (2)). Here, we take accretion rates of the sMBH during the interval of $\Delta t_{\rm cav}$ as a constant as an averaged one given by Equation (2). The temporal profiles of the $L_{\rm BZ}$ depend on the evolution of density and temperature of the cavity; we will investigate this issue in the future.

The observational appearance of the BZ power release depends on two classes of factors: (1) the proceeding of the cavity formation driven by episodic accretion onto sMBH and (2) the dynamical interaction between the jet and the SMBH-ADAF, both of which determine the temporal profiles of the flickerings. These temporal processes make it very difficult to estimate the time-dependent Lorentz factor of the jets. Considering the difficulties in this paper, we consider two possible outcomes for the relativistic ejecta: (1) they are partially choked and exhibit subrelativistic wisps after emerging; (2) they can penetrate the entire SMBH-ADAF resulting in the appearance of superluminal blobs. Without details of the jet dynamics, a flickering apparently appears when a jet can penetrate the SMBH-ADAF through a length of the ADAF, and the Lorentz factor reaches

$$\Gamma\approx\frac{L_{\rm BZ}\Delta t_{\rm cav}}{\Delta M_{\rm j}c^2}\approx8.5\,\alpha_{0.1}^{-1}x_{\rm j,1}^{-2}j_\bullet^2r_1^2\left(\frac{\ell_j}{H_{\rm p}/3}\right)^{-1}, \quad (14)$$

where $\Delta M_{\rm j}=\pi X_{\rm b}^2\ell_{\rm j}n_{\rm e}m_{\rm p}$ is the mass of the jet, $x_{\rm j,1}=X_{\rm b}/10r_{\rm g}$ is the jet radius obtained from the analytical solution of the BZ process (e.g., Chen & Zhang 2021), $r_{\rm g}$ is the gravitational radius of the sMBH, and $\ell_{\rm j}$ is its length. This is the average Lorentz factor of the jet, which is similar to that of radio-loud AGNs (Ghisellini et al. 1993). After the Lorentz factor falls below a critical one, the flickering disappears (since the

Doppler boosting greatly weakens). Moreover, beyond this length, the jet experiences significant deceleration. Considering observational evidence of subrelativistic ejecta from nuclear regions of the Galactic Center (e.g., Rauch et al. 2016) and other LLAGNs (Middelberg et al. 2004), we choose case (1) that this jet is slowed down at $H_{\rm p}/3$ from relativistic states to subrelativistic ones. The bulk Lorentz factor of the jet is similar to that of blazars (Ghisellini et al. 1993). It should be noted that the Lorentz factor is fully independent of the sMBH because both $L_{\rm BZ}$ and $\Delta M_{\rm j}$ are proportional to the square of the sMBH masses. From Equation (14), we know the choked length is a significant fraction of the thickness of the SMBH-ADAF. The appearance of the jet strongly depends on the location of the sMBH as the result of SMBH-ADAF density. If the sMBH is located at around $20\,R_{\rm g}$ or so, the jet is capable of penetrating the entire SMBH-ADAF, showing superluminal motions of blobs. Considering the Doppler boosting effects, we have the observed luminosity of the jet inside the ADAF

$$L_{\rm jet} = L_{\rm BZ}\mathcal{D}^4 = 1.92\times10^{36}\,\alpha_{0.1}^{-1}j_\bullet^2\mathcal{D}_{10}^4\dot{\mathscr{M}}_{\rm p,\bar{3}}q_{\bar{5}}^2\left(\frac{M_6}{4}\right){\rm erg\ s^{-1}}, \quad (15)$$

where $\mathcal{D}_{10}=\mathcal{D}/10$, $\mathcal{D}=1/\Gamma(1-\beta_{\rm j}\cos\theta)$ is the Doppler factor, $\Gamma=1/(1-\beta_{\rm j}^2)^{1/2}$ is the Lorentz factor, $\beta_{\rm j}=v_{\rm j}/c$ is the jet velocity, and $\cos\theta$ is the cosine of the viewing angle. Here, we take $\theta=5.^\circ7$, and $\Gamma=8.5$, for $\mathcal{D}=10$. We note that the SMBH-ADAF is optically thin ($\tau_{\rm es}\sim0.008\ll1$), which allows observers to see the emissions from the relativistic part of the choked jets. The choked part of the jet becomes ejecta, which carries the rest of the BZ power and can emerge with a subrelativistic velocity of

$$\frac{v_{\rm eje}}{c}\approx\left(\frac{\xi L_{\rm BZ}\Delta t_{\rm cav}}{\Delta M_{\rm j}c^2}\right)^{1/2}=0.53\,\xi_{0.1}^{1/2}\alpha_{0.1}^{-1/2}j_\bullet x_{\rm j,1}^{-1}r_1\left(\frac{\ell_{\rm j}}{H_{\rm p}}\right)^{-1/2}, \quad (16)$$

where $\xi_{0.1}=\xi/0.1$ is the fraction of the BZ power remaining after the jet radiates its most part of the BZ power. This is consistent with the wisps in Sgr A* observed by Rauch et al. (2016). If the relativistic ejecta is entirely choked, the emissions could be too faint to detect. In such a case, no flickering appears.

As a result of the continual heating of sMBH-outflows, the accumulated energies give rise to a flare. Therefore the number of flickerings can be estimated by considering the cooling and cavity timescales before a flare happens in the presence of the instability of the SMBH-ADAF (the regions with a radius of $R_\bullet\sim H_{\rm p}$ described by Equation (10)). It follows from

$$N_{\rm flick}=\frac{\Delta t_{\rm cool}}{\Delta t_{\rm cav}}\approx7.4\left(\frac{\Delta t_{\rm cool}}{5.6\ {\rm hr}}\right)\left(\frac{\Delta t_{\rm cav}}{45.9\ {\rm minutes}}\right)^{-1}. \quad (17)$$

This indicates that flares always appear after about a couple of flickerings. This is an important feature to observationally test the present model. Indeed, this is consistent with observations of Sgr A* (see the Spitzer data of Boyce et al. 2022).

The $L_{\rm BZ}$ (Equation (13)) is converted into the nonthermal emissions from the relativistic jet. Internal shocks are formed due to successive ejecta from the sMBH-ADAF whereas external shocks are formed through the collisions between the jet and the SMBH-ADAF. This process is similar to gamma-ray bursts (e.g., Mészáros 2002). Moreover, the jet is undergoing mass-loading processes when it penetrates through the SMBH-ADAF. The temporal profiles of flickerings, as discussed previously, depend on both the Bondi accretion processes and the propagation of the relativistic jet inside the SMBH-ADAF. Details of the temporal profiles of the flickerings can be further understood by numerical simulations. We would like to point out the diversity of the sMBH-driven phenomena. In the high-$\dot{\mathscr{M}}$ SMBH-ADAFs, the jet is seriously choked so that the Doppler boosting effects are too faint to see the flickerings; however, the sMBH-outflows can still trigger flares through viscous instability.

2.3. SED of the Jet

In order to calculate the SED from the relativistic jet, we have to know the magnetic fields and energy distributions of nonthermal electrons. The one-zone model is the simplest, in which nonthermal electrons, magnetic fields, and bulk Lorentz factor of the jet are homogenous, and it is often employed for the canonic SED of blazars (e.g., Inoue & Takahara 1995). In the current case of sMBH-ADAF, the magnetic fields are so strong (than that of blazars) that SEDs generated by this model have too high-frequency cutoff even in the NIR bands (see Figure 3 for smaller index m). Therefore, we employ a simplified version of the inhomogeneous model of jets (Ghisellini et al. 1985; Georganopoulos & Marscher 1998). Since both geometries of the jet and its magnetic fields are poorly understood, we consider a simple cone of the jet, and its cross-sectional radius increases with height ($z_{\rm j}$) as $X_{\rm j}=X_0(z_{\rm j}/z_0)^m$, where X_0 is the jet radius at the base z_0, and the index m describes the geometry. In light of the self-similar solution (e.g., Narayan & Yi 1995)

$$B_{\rm disk}=2.9\times10^4\,\alpha_{0.1}^{-1}(1-\beta_{\rm s})^{1/2}\dot{\mathscr{M}}_{\rm p,\bar{3}}^{1/2}x_1^{-5/4}\left(\frac{M_6}{4}\right)^{-1/2}{\rm G}, \quad (18)$$

where $\beta_{\rm s}$ is the magnetization parameter of the sMBH-ADAF, $x_1=X_0/10\,r_{\rm g}$ is the radius of the sMBH-ADAF. We assume that the poloidal magnetic fields of the jet (i.e., $B_\perp$ in Equation (12)) at its base follow the sMBH-ADAF, and have

$$B_{\rm j}=B_{\rm disk}\left(\frac{X_{\rm j}}{X_0}\right)^{-2}=B_{\rm disk}\left(\frac{z_{\rm j}}{z_0}\right)^{-2m}, \quad (19)$$

based on a simple conservation of the magnetic fluxes. In this paper, we skip the details of electron acceleration, which involve many processes (formation and diffusions of shocks, energy gains, and losses during the propagation of the jet through the SMBH-ADAF; see details in Blandford & Eichler 1987). In the present paper, we assume a power-law distribution of the electrons as

$$N_{\rm e}=N_0\gamma^{-s}\left(\frac{z_{\rm j}}{z_0}\right)^{-2m}\quad{\rm for}\ \gamma_{\rm min}\leqslant\gamma\leqslant\gamma_{\rm max}, \quad (20)$$

where γ is the Lorentz factor of nonthermal electrons, $\gamma_{\rm min,max}$ are the minimum and maximum, respectively, s is the electron index, $N_0=(s-1)N_{\rm tot}/\gamma_{\rm min}^{1-s}[1-(\gamma_{\rm max}/\gamma_{\rm min})^{1-s}]$, and $N_{\rm tot}$ is the number density of relativistic electrons. The factor

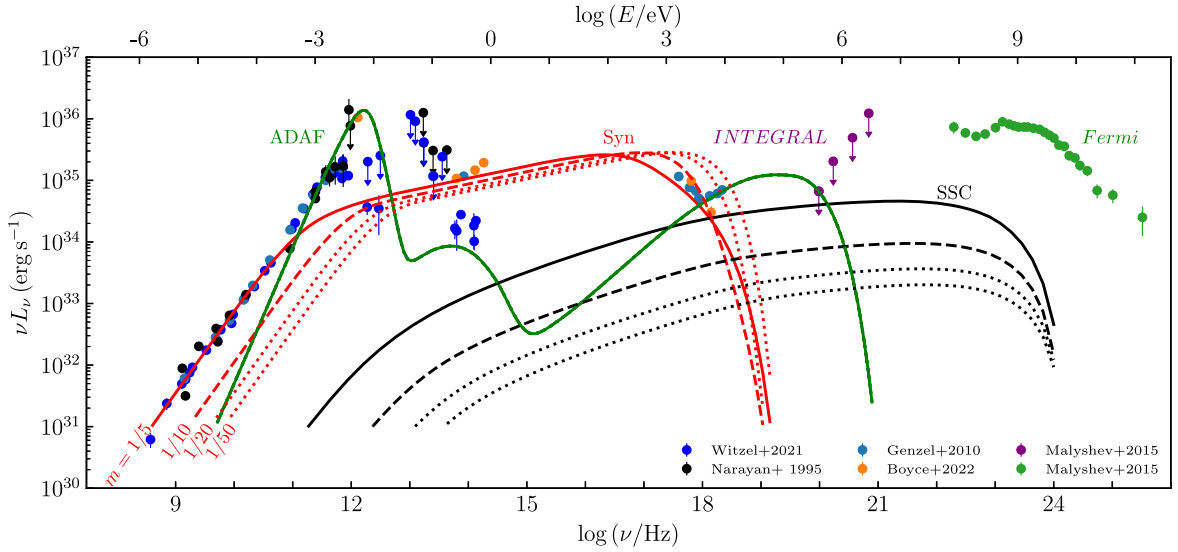

Figure 3. The overall spectral energy distribution of Sgr A* from radio to TeV bands. We get the accretion rates of the SMBH from the averaged SED. Curves are marked by the same color words. Syn: synchrotron radiation from the relativistic jet developed by the sMBH accretion. ADAF-EC: external IC (EC) of SMBH-ADAF photons. SSC: synchrotron self-Compton scattering. Narayan & Yi (1995) collected early radio data (we omit these references). INTEGRAL and Fermi data are from Malyshev et al. (2015). When $m \to 0$, the inhomogeneous model becomes one-zone model.

$(z_j/z_0)^{-2m}$ results from the mass conservation in a continuous jet. We take $\gamma_{\rm min,max}$ as constants along the jet. When $m \to 0$, the present model tends to the one-zone model.

Emissions from the jet in its comoving frame can be expressed by

$$L_\nu^{\rm Syn} = \int_{z_0}^{\ell_j} \pi X_j^2 j_\nu^{\rm Syn}(z_j) dz_j; \text{ and } L_\nu^{\rm IC} = \int_{z_0}^{\ell_j} \pi X_j^2 j_\nu^{\rm IC}(z_j) dz_j, \quad (21)$$

where $j_\nu^{\rm syn}$ and $j_\nu^{\rm IC}$ are the synchrotron and IC emissivities, respectively. We then transform these into the observer's frame in order to compare with observations (e.g., Lind & Blanford 1985). We neglect the synchrotron self-absorption since most photons are radiated from the sides of the jet and are beamed by the bulk motion of the jet, even if the optical depth is larger than unity along the jet direction. We neglect the pair production of the IC photons. The total number of nonthermal electrons ($N_{\rm tot}$) is constrained by $L_{\rm BZ} = \int_{z_0}^{\ell_j} \pi X_j^2 dz_j \int_{\nu_1}^{\nu_2} (j_\nu^{\rm Syn} + j_\nu^{\rm IC}) d\nu$, where ν_1 and ν_2 are frequencies of the synchrotron radiation and IC. We use the standard formulations of synchrotron self-Compton (SSC) emissions and IC Blumenthal & Gould (1970), for the simple SED of the jet. We approximated it with an isotropic radiation field. The ADAF is taken to be a point source with a luminosity $L_{\rm ADAF}$, and an averaged energy density of $u_{\rm ADAF} = L_{\rm ADAF}/4\pi R^2 c$ at a distance R. In the comoving frame, the relativistic jet receives an energy density of the SMBH-ADAF given by $U_{\rm ADAF} \approx \Gamma^2 u_{\rm ADAF}$, which is the external source of seed photons (Sikora et al. 1994). We ignore external Compton scattering since $U_{\rm B}/U_{\rm ADAF} \sim 10^6$ holds in the current parameters of the jet. We omit all the formulations in this paper. Generally, there are two peaks of SEDs arising from synchrotron and IC, respectively.

We take $M_6 = 4.0$, $\dot{\mathscr{M}}_{\rm p,\bar{3}} = 1$, and $\alpha_{0.1} = 1$. Following Narayan & Yi (1995), Manmoto (2000), we take the electron heating coefficient $\delta = 0.03$ in this paper; though, it may have large uncertainties (e.g., Yuan et al. 2003). We calculate the SMBH-ADAF SED for $\beta_{\rm p} = (0.99, 0.5, 0.35)$. Figure 2 shows the results. Generally, SEDs of the SMBH-ADAF are consistent with those of Manmoto (2000). The first peak of the SMBH-ADAF arises from synchrotron radiation of the Maxwellian distributions of hot electrons, and the peak shifts and powers vary with $\beta_{\rm p}$. Comptonization of the hot electrons results in the second peaks, and the bremsstrahlung contributes to the last peak with a cutoff related to the maximum temperatures of electrons.

For parameters of the jet, we take $x_{\rm j,1} = 1$, $\ell_{\rm j} = H_{\rm p}/3$, $\Gamma = 8.5$, and $\theta = 5\overset{\circ}{.}6$. We fix the jet location at the radius of $x_1 = 1$. For a jet with $m = 1/5$, the top of the jet $z_{\rm j,\ top} = \ell_{\rm j} \approx 10^{12}$ cm, $\ell_{\rm j}/z_0 \sim 10^4$, we have $X_{\rm j} \approx 7\, X_0$, and the magnetic fields decay by a factor of 50 along the jet height. The free parameters are $\gamma_{\rm min}$, $\gamma_{\rm max}$, s, m, and $\beta_{\rm s}$. We take $s = 2.0$, $\gamma_{\rm min} = 1$, and $\gamma_{\rm max} = 10^3$, and $m = 1/5$ for the theoretical SEDs. We adjust $\beta_{\rm s}$ in order to show the role of the magnetic fields in the jet SED. Since we keep the power of jets as a constant ($L_{\rm BZ}$), we adjust electron numbers for the dependence of the SED on magnetic fields, $\gamma_{\rm min,max}$, $\beta_{\rm s}$, s, and m. The synchrotron emissions shift toward lower frequencies with increases of $\beta_{\rm s}$ because B decreases. As shown in Figure 2, the synchrotron emissions from the jet just supplement the deficits of the SEDs from SMBH-ADAFs depending on the maximum energies of electrons ($\gamma_{\rm max}$), in particular, contributing to infrared to soft X-ray bands. The SED of the jet shifts toward low frequency with decreases of m. This results from the fact that magnetic fields decrease along the jet height with m. When m tends to zero, the jet tends to the one-zone model.

IC of synchrotron photons is significant compared with the power of the synchrotron emissions. It strongly depends on the magnetic fields of the sMBH-ADAF. In $\beta_{\rm p,s} = 0.99$ case (weak magnetic field) as shown in Figure 2, the self-inverse Compton power is comparable with that of the synchrotron radiation. This significantly contributes to γ-ray bands but relies on $\gamma_{\rm max}$. With increases of magnetic fields ($\beta_{\rm s}$ decreases), the IC power decreases dramatically.

For a simple treatment, we take a constant bulk Lorentz factor of the jet in the present model. Dynamical interaction with the SMBH-ADAF will slow down the jet. A self-consistent treatment

of this is necessary (e.g., Contopoulos & Kazanas 1995) since the fully parameterized model of inhomogeneous jets could be useful to explore the SEDs of the sMBH-driven jets like in blazars (Georganopoulos & Marscher 1998). Moreover, it is necessary to explore the time-dependent model of the relativistic jets for the temporal profiles of the light curves. This is left for future research. We would like to point out that the BZ process can also occur in the SMBH-ADAF if the SMBH is rotating fast enough. In such a context, emissions of the sMBH-ADAFs are overwhelmed by the SMBH-ADAFs. BL Lac objects and face-on radio galaxies (Fannaroff–Rilley I radio galaxies) are known to contain ADAFs, which power relativistic jets (Cao & Rawlings 2004; Sikora et al. 2007; Tadhunter 2016). Actually, LLAGNs often show large radio-loudness (e.g., Ho 2002) but lack powerful jets (e.g., Middelberg et al. 2004), implying that the SMBHs in most LLAGNs are nonrotating. There is no evidence that the BZ process works in SMBH-ADAF of Sgr A*, which only shows subrelativistic wisps discovered by Rauch et al. (2016). If we apply Equation (13) to Sgr A*, the BZ power will be around 10^{40} erg s^{-1} if $j_\bullet \sim 1$, which is much more luminous than the observation of the total emissions of Sgr A*. The central SMBH is thus expected to be very slowly spinning in Sgr A*. This is favored by the presence of two misaligned young stellar disks in light of the LenseThirring effects (Fragione & Loeb 2022); though, Event Horizon Telescope (EHT) observations favor $j_\bullet \gtrsim 0.5$ (EHT Collaboration et al. 2022). Moreover, the observational fact that there are two counter-rotating young stellar disks within 30″ regions (about 1 pc) of the Galactic Center identified by SINFONI Intergral Field Unit at the Very Large Telescope (von Fellenberg et al. 2022) directly indicates random accretion onto the central SMBH, making the SMBH spin very low (Wang et al. 2009; Volonteri et al. 2013). Independent evidence for random accretion onto the central SMBH is provided by Atacama Large Millimeter/submillimeter Array that two counter-rotating disks of gas in NGC 1068 have been found by Impellizzeri et al. (2019). Cancellations of the AM of gas ($\lesssim$10 pc nuclear regions) finally drive extremely high accretion rates of the SMBH, which likely leads to a super-Eddington growth of the SMBH.

2.4. Gravitational Waves

In this paper, an sMBH orbiting the central SMBH is an excellent extreme mass ratio inspiral (EMRI). We assume that the EMRI follows a circular orbit. This can be justified by the decaying of ellipticity due to radiations of GWs. According to Peters (1964), we have the circularization timescale $t_{\rm E} = (d\ln e/dt)^{-1}$, where e is the ellipticity of the initial orbit, if the GWs radiations govern the evolution of the EMRI orbit. A highly elliptical orbit of an EMRI will be circularized with $t_{\rm E} = (d\ln A/d\ln e)t_{\rm GW} \approx (1-10)t_{\rm GW}$, from an initial elliptical orbit of $e_0 = 0.9$, from $A = 100\,R_{\rm g}$, where A is the separation of the EMRI, $d\ln A/d\ln e = 12[1 + (73/24)e^2 + (37/96)e^4]/19(1-e^2)[1 + (121/304)e^2]$. We expect that the sMBH undergoes rapid circularization of orbits and reaches a circular orbit at $A = 10R_{\rm g}$. Their strain amplitudes and frequency of GWs from the EMRI are given by

$$h_{\rm s} = \left(\frac{128}{15}\right)^{1/2}\frac{(GM_{\rm c})^{5/3}}{c^4 d_{\rm L}}(\pi f)^{2/3} = 7.6\times10^{-17}\,d_{10\,\rm kpc}^{-1}a_1^{-1}q_{\bar{5}}\left(\frac{M_6}{4}\right), \quad (22)$$

where $M_{\rm c} = (M_{\rm p}M_{\rm s})^{3/5}(M_{\rm p}+M_{\rm s})^{-1/5} = q^{3/5}(1+q)^{-1/5}M_{\rm p}$ is the chirping mass, and

$$f = \frac{2}{P_{\rm orb}} = 0.5(1+q)^{-1/2}a_1^{-3/2}\left(\frac{M_6}{4}\right)^{-1}\ {\rm mHz}, \quad (23)$$

where $P_{\rm orb}$ is the orbital periods, $d_{10\,\rm kpc} = d_{\rm L}/10\,{\rm kpc}$ is the distance to observers, $a_1 = A/10R_{\rm g}$, and $P_{\rm orb}$ is its orbital period. The GWs are in the bands of Laser Interferometer Space Antenna (LISA), and the other two space missions of Taiji (Hu & Wu 2017), Tianqin (Luo et al. 2016), whose thresholds ($h_{\rm s} \approx 10^{-20}$) are much lower than strains of the present EMRI. The decaying timescale of the circular orbit is (e.g., Peters 1964)

$$t_{\rm GW} = \frac{A}{dA/dt} = \frac{5a^4}{64q(1+q)}\left(\frac{R_{\rm g}}{c}\right) \approx 48.8\,a_1^4 q_{\bar{5}}^{-1}\left(\frac{M_6}{4}\right){\rm yr}, \quad (24)$$

which is a feasible timescale to witness an EMRI merger. We note that this timescale is very sensitive to the separation of the EMRI, and expect GRAVITY/VLTI to make a precise measurement of the orbit from the flares in Sgr A*.

In summary, an sMBH residing in the ADAF of the central SMBH has to undergo an episodic Bondi accretion governed by its strong feedback. A cavity is formed by the outflows from the accretion. During the accretion, a relativistic jet is formed by the BZ mechanism, showing quasi-periodic flickerings (jet emissions) from the sMBH-ADAF. Accumulations of the outflow energies will trigger the viscous instability of the SMBH-ADAF and generate a flare subsequently. Milli-Hz GWs are radiated by the EMRI, which is strong for the detection of the designed space missions. Table 1 lists all the parameters involved in this model. Given an sMBH-SMBH system in the ADAF state, the temporal properties of the system can be predicted for quasi-periodic flickerings and flares.

2.5. Discussions

In this paper, the AMS plays a role in perturbations of the SMBH-ADAF while the latter is in a relatively stationary state. Flickerings are a tiny fraction of the SMBH-ADAF radiation, but the flares are stronger than the former. Therefore, light curves are expected to show as depicted by the right panel of Figure 1, where flares and flickerings are thus just superposed on a relatively stationary radiation flux. If the sMBH is nonrotating (or its rotation is not fast enough), flickerings disappear (the lower panel). We denote this type-A light curve, and type-A1 and type-A2 for the cases with and without flickerings, respectively. Actually, Sgr A* shows the type-A light curves; see Figure 1 in Boyce et al. (2022), NGC 4151 (see Figure 4 in Chen et al. 2023), and NGC 5548 (see Figure 3 of Li et al. 2016).

For high-q system, however, feedback of the sMBH accretion to the SMBH-ADAF is not a perturbation. Large zones of the SMBH-ADAF will be broken, and giant flares are expected from these high-q systems. We hence anticipate an upon-down style of light curves. This denotes type-B light curves. Similar to type-A curves, type-B curves are distinguished as type-B1 and type-B2 with and without flickerings, respectively. Actually, Arakrian 120 has exhibited type-B light curves over the last 20 yr (Li et al. 2019). Collections of

Table 1
Parameters of the sMBH-SMBH System (EMRI)

Parameters	Meanings
Parameters describing the system given by the initial conditions	
$M_{\rm p,s}$	Masses of the SMBH and sMBH, respectively; the mass ratio is defined by $q = M_{\rm s}/M_{\rm p}$
$\dot{\mathscr{M}}_{\rm p,s}$	Dimensionless accretion rates of the SMBH and sMBH in units of $L_{\rm Edd}/c^2$, respectively
$R_{\bullet}$	sMBH location radius at the SMBH-ADAF (or A: the separation between sMBH and SMBH)
Parameters of accretion physics	
$\alpha_{\rm p,s}$	Viscous parameters of the SMBH and sMBH
$\beta_{\rm p,s}$	Magnetization parameters of the SMBH and sMBH
$\eta_{\rm out}$	Efficiency of outflows driven by sMBH-ADAF
Derived parameters of the system for observations of flickerings and flares	
$R_{\rm cav}$	Radius of the cavity created by the SMBH-ADAF outflows
$\Delta t_{\rm cav}$	Formation timescale of the cavity as the quasi-periods of flickerings
$\Delta t_{\rm cool}$	Cooling timescale of the SMBH-ADAF as outburst timescales of flares
$R_{\rm flare}$	Radius of the cavity zones generating flares from the SMBH-ADAF
$L_{\rm BZ}$	Blandford–Znajek power of the sMBH
$j_{\bullet}$	Specific angular momentum of the sMBH
Γ	Lorentz factor of the relativistic jet developed by the sMBH-ADAF
$v_{\rm eje}$	Subrelativistic velocity of the choked part of the relativistic jet
$N_{\rm flick}$	Numbers of flickerings triggering a flare
$h_{\rm s}$	Strains of the gravitational waves from the sMBH-SMBH binary system
f	Frequency of the gravitational waves
$t_{\rm GW}$	Timescales of orbital decays due to gravitational waves
Parameters of the relativistic jet (assumed in this paper)	
$X_{\rm j}$	Cross-sectiobal radius of the jet; X_0 is the initial radius
$\ell_{\rm j}$	Length of the jet; z_0 is the initial height of the jet; $z_{\rm j}$ is jet height
s	Distribution index of nonthermal electrons of the relativistic jet ($\propto \gamma^{-s}$)
m	Geometric index of the cross-sectional radius of the jet versus its height ($X_{\rm j} \propto z_{\rm j}^{m}$)
$\gamma_{\rm min,max}$	Minimum and maximum Lorentz factors of nonthermal electrons

low-$\dot{\mathscr{M}}$ AGN light curves can test this classification, but it needs homogeneous light curves spanning longer than 20–30 yr. We emphasize that these classifications of light curves are only valid for the case that the central SMBHs have ADAFs, and the physics for SMBHs with high-$\dot{\mathscr{M}}$ should be reconsidered separately.

In the present study, we set the typical values of an AMS with a mass of $\sim 40 M_{\odot}$ at $10\,R_{\rm g}$ around the central SMBHs of $4 \times 10^6 M_{\odot}$ for the Galactic Center. The resultant properties of the AMS depend on its mass, location, and the SMBH-ADAF accretion rates. The BZ power is proportional to $M_{\rm s}^2$ (see Equation (13)). The fates of the relativistic jet depend on the SMBH-ADAF. It either penetrates the ADAF and shows superluminal motion outside the nucleus or is partially choked by the ADAF giving rise to subrelativistic ejecta from the nucleus (see Equation (16)). If the BZ power is not strong enough compared with the SMBH-ADAF damp, flares still occur but without flickerings. Moreover, the sMBH has a Keplerian rotation velocity of $v_{\rm rot} \sim c/3$ at $R_{\bullet} \sim 9\,R_{\rm g}$, emissions from the jet developed by the sMBH-ADAF could be modulated by transverse Doppler boosting. Additionally, general relativistic effects should be employed for temporal profiles of flickerings.

Shocks formed by the dynamic interaction between sMBH-outflows and SMBH-ADAF can accelerate electrons and generate nonthermal emissions. As a simple estimation, the kinetic power of the shocks is around $L_{\rm out} \approx 8 \times 10^{33}\,{\rm erg\,s^{-1}}$, and about 10% of $L_{\rm out}$ will be channelled into nonthermal electrons (e.g., Blandford & Eichler 1987) and contribute to multiwavelength continuum. This component causes complicated behaviors of variabilities of the system. This topic remains a future issue.

We assume that the global SMBH-ADAF is stationary. It is then expected to exhibit quasi-periodicity of flickerings and flares from the system. However, the reality could be complicated. For example, $\dot{\mathscr{M}}_{\rm p}$ is a function of the radius of SMBH-ADAF (Blandford & Begelman 1999), and due to clump accretion (Wang et al. 2012a), the periodicity of flickerings and flares dramatically decreases and even becomes random sometimes. For example, NGC 5548 shows preliminary periodicity in its long-term light curves with flickerings (Li et al. 2016), but the periodicity of flickerings is usually verily twinkled by showing 3–4 cycles.

Finally, we would like to point out the key tests of the present model. LISA detections around 2030 can more accurately determine the EMRI system for a concluding remark. Before the LISA era, GRAVITY+/VLTI observations of Sgr A* can provide more solid and accurate loci of NIR-flares from increasing observations to obtain the orbiting radius of flares, on which the merger timescale sensitively depends. The current error bars of the flare's loci are still quite large (about 30%–50%). Flickering numbers associated with flares are another feature of the EMRI system, and we anticipate acquiring more data for high statistics of the flares and flickerings.

3. Application to Sgr A*

As a preliminary practice of the present model, we apply it to Sgr A*, which is the best-studied low-luminosity system. An early extensive review on this object can be found for general properties in Genzel et al. (2010). It has been extensively observed through multiwavelength campaigns during the last 20 yr and shows a diversity of variability properties (see a brief summary of observations in Witzel et al. 2021; Boyce et al. 2022; von Fellenberg et al. 2023). The powerful astrometric measurements of GRAVITY/VLTI provide an exciting ring of locations of flares during the last 4 yr. The ring is phenomenologically explained as a moving hot spot around the SMBH. It has a radius of $R_{\bullet} = 8.9^{+1.5}_{-1.3}\,R_{\rm g}$ and is rotating with the azimuthal speed of near Keplerian motion (see also their Figure 7 in Gravity Collaboration 2023a). A hot spot due to magnetic reconnection in the SMBH-ADAF has been suggested for flares in Sgr A* (see references subsequently cited), but an orbiting sMBH can explain the properties of flares and flickerings as an alternative model. Actually, the light curves show that flickerings and flares are superposed on relatively stationary fluxes (see Spitzer, Chandra light curves; Boyce et al. 2022), implying that they are perturbations of the SMBH-ADAF. This indicates that Sgr A* should be classified as one type-A2 object.

3.1. Accretion Rates

The SMBH mass is accurately measured $M_{\rm p} = 4.3 \times 10^6\,M_{\odot}$ (see the latest values given by Gravity Collaboration 2022). The classical ADAF model was first applied to explain SED (from radio to hard X-rays) of Sgr A* (Narayan et al. 1995), which was revised by including fully general relativistic effects (e.g., Manmoto 2000; Li et al. 2009). Figure 3 shows the global SED from radio to TeV bands. We use the classical ADAF model (e.g., Li et al. 2009) to get the accretion rates for discussions on the sMBH properties. γ-ray emissions through hot proton–proton collisions in the ADAFs have been suggested by Mahadevan et al. (2003), but it is only a small fraction of the total ADAF emissions (Oka & Manmoto 2003) that is much below the Fermi observations as shown by Figure 3. For Sgr A*, there are only three free parameters in this model, accretion rates ($\dot{\mathscr{M}}$), viscosity (α), and magnetization parameter ($\beta_{\rm p}$). We take the SMBH mass measured by GRAVITY (Gravity Collaboration 2022), and fix the typical values of the magnetization parameter of $\beta = 0.35$, and the viscosity of $\alpha = 0.1$. We find $\dot{\mathscr{M}}_{\rm p} = 10^{-3}$ for a global fitting (the green line for most points except for flaring points in Figure 3), which agrees with previous results of Manmoto (2000).

It has been also suggested that the X-ray flare emission is due to synchrotron radiation (Dodds-Eden et al. 2009; Barriére et al. 2014; Ponti et al. 2017) although it has been also interpreted as IC upscattered photons by the mildly relativistic, nonthermal electrons (Markoff et al. 2001; Yuan et al. 2003; Yusef-Zadeh et al. 2009; Ball et al. 2016). It is obvious that the Fermi γ-ray emissions (Chernyakova et al. 2011; Malyshev et al. 2015) are much beyond the scope of the SMBH-ADAF continuum emissions, but they have a luminosity of $10^{36}\,{\rm erg\,s^{-1}}$ from 100 MeV to 500 GeV. It has been suggested by Malyshev et al. (2015) that the Fermi-detected bump originates from IC by high-energy electrons in extensive regions, indicating an extra source of nonthermal emissions in Sgr A* (see the possibilities discussed in Cafardo & Nemmen 2021). It is not our goal to extensively explore the delays among the multiwavelength variations, but we explain the major properties of flickerings and flares and suggest future tests of the present model.

3.2. Flares and Quasi-periodic Flickerings

NIR flares are more common on timescales of hours or so. X-ray flares often accompany NIR ones, but sometimes do not (Boyce et al. 2022). Several kinds of models are suggested to explain multiwavelength variations, such as the popular magnetic reconnection events (e.g., Dexter et al. 2020; Mellah et al. 2023), nonthermal electrons in a jet (Markoff et al. 2001; Yuan et al. 2003), sudden instabilities of the MHD disk (e.g., Chan et al. 2009), or other stochastic processes in the ADAFs (see more references listed by Boyce et al. 2022). The most interesting is that Genzel et al. (2003) discovered quasi-periodic flickerings of ~17 minutes, which were superimposed to a flare in NIR bands during one epoch of 2002 (but see different results in other epochs of Do et al. 2009). X-rays of XMM-Newton observations show the similar periods (Aschenbach et al. 2004; Eckart et al. 2006). This quasi-periodic flickering (at 4 μm) has been confirmed by the Spitzer observations (Boyce et al. 2022). It has been argued that the appearance of the flickering quasi-periodicity ($17 \sim 40$ minutes) depends on epochs (see a summary of the quasi-periodicity in Genzel et al. 2010); though, Do et al. (2009) thought of the red-noise roles. The quasi-periodicity of flickerings has been suggested to arise from the quasi-periodic structure of plasma as hot spots (e.g., Dexter et al. 2020; Aimar et al. 2023; Lin et al. 2023; Mellah et al. 2023) or an expanding hot spot (Michail et al. 2023). However, this kind of model involving magnetic reconnections should explain why the flares constantly happen at the same radius (namely, $\sim 9R_{\rm g}$) since the reconnections randomly happen somewhere inside the SMBH-ADAF. Second, one orbiting star as a pacemaker is suggested by Leibowitz (2021) for the periodicity of NIR and X-ray flares. A hidden BH with a mass of $\sim 10^4 M_{\odot}$ has been suggested by Naoz et al. (2020); however, the BH with $\gtrsim 10^3 M_{\odot}$ has been ruled out by precise measurements of S2 orbits (Gravity Collaboration 2023b; Will et al. 2023). Recently, Gravity Collaboration (2023a) maps the loci of the flare's locations during the last 4 yr and finds that the loci are consistent with the Keplerian orbits at a distance of $\sim 9\,R_{\rm g}$ from the central SMBH well determined by the S2 star. For the magnetic reconnection model of the hot spots, the question of how to keep them in similar loci remains open. This new solid evidence supports a rigid body around the central SMBH. We suggest here an sMBH is orbiting around the SMBH in Sgr A* in charge of flares and quasi-periodic flickering.

For simplicity, we assume the sMBH spin axis to be perpendicular to the SMBH-ADAF equatorial plane. Since the quasi-periods are about 17–40 minutes (we take the mean quasi-period is bout 30 minutes), we have the accretion rates of $\dot{\mathscr{M}}_{\rm s,\tilde{6}} \approx 2.0$ from Equation (2), $\dot{\mathscr{M}}_{\rm p,\tilde{3}} = 1.0$, $r_1 = 0.9$, and $M_6 \approx 4.3$. We obtain the quasi-periods of $\Delta t_{\rm cav} \approx 42.1\,\alpha_{0.1}^{-1}$ minutes from Equation (7), which is in agreement with observed quasi-periods (Genzel et al. 2010) if $\alpha_{0.1} \approx 1.5 \sim 2$ slightly fluctuates. Flares are generated with $\Delta t_{\rm vis} \approx 10.1$ hr, which is well consistent with the observed, namely, there are a few flares per day. The SED of the jet is shown in Figure 3, where we take $s = 2.6$, $\beta_{\rm s} = 0.35$, $\gamma_{\rm min} = 2.0$, $\gamma_{\rm max} = 10^3$, and $m = 1/5,\ 1/10,\ 1/20,\ 1/50,$

respectively, for the 1–100 GHz bands, NIR bands, and soft X-rays. The most significant effects are observed in the SED at low frequencies. The well-known 1–100 GHz emissions beyond the SMBH-ADAF, which are usually explained by a relativistic jet from the SMBH-ADAF lacking of choke effects (Markoff et al. 2001; Yuan et al. 2003; Yusef-Zadeh et al. 2009; Ball et al. 2016), can be reasonably explained by the present model. Ejecta from Sgr A* has been observed but it is subrelativistic (Rauch et al. 2016). The present model is consistent with the ejecta. It should be mentioned that some parameters degenerate in fitting SED, for example, $\gamma_{\rm min}$, m, and $\beta_{\rm s}$. The most important thing is to identify this EMRI system at this stage, and we leave it for the future to make a self-consistent model for jet emissions. However, the Fermi SED cannot be explained by the present jet model. We agree that Fermi γ-ray emissions are from extensive regions since no evidence is found for γ-ray variability (e.g., Cafardo & Nemmen 2021).

The simple model can, in principle, explain the major properties of the flares and quasi-periodic flickerings. We note that the extensive multiwavelength observations show complicated behaviors of variations, such as delays among radio, NIR, and X-ray bands. Although some attempts have been made (e.g., Okuda et al. 2023), we will apply the present model to Sgr A* in more sophisticated treatments to explain variabilities and polarizations by including inner shocks and external shocks of the jet. Moreover, wisps with subrelativistic velocity ($\sim 0.4c$) from Sgr A* have been discovered by Rauch et al. (2016), which could be the remnant, i.e., $\xi L_{\rm BZ}$, of the relativistic jets slowed down by interaction with surrounding medium from the sMBH-ADAF. Indeed, LLAGs often show subrelativistic ejecta (e.g., Middelberg et al. 2004). A damped jet model will be discussed for this issue in a separate paper. A few points would be stressed as follows.

First, the nonthermal emissions from the relativistic jet can be, in practice, tested by a multiwavelength campaign of simultaneously monitoring Sgr A*. In particular, the GHz radio and soft X-rays correlations (synchrotron emissions), and with Fermi γ-ray bands (external IC) are the keys to testing the present model of the sMBH. Hard X-rays may be mainly contributed by the SMBH-ADAF. Second, the emissions from the shocks formed by the outflows and SMBH-ADAF also contribute to emissions in some bands from radio to X-rays (even soft γ-rays). This makes the tests not so direct. Okuda et al. (2023) made an extensive analysis of the multiwavelength correlations, but they draw conclusions that the multiwavelength continuum has complicated originations. The correlations may depend on the states of Sgr A*. Third, optical and UV bands are the key bands of testing SMBH-ADAF model, but it is impossible to have observations owing to the heavy extinctions of the Galactic Center. Fortunately, International Gamma-Ray Astrophysics Laboratory (INTEGRAL, 15 keV–10 MeV) has a sensitivity ($\sim 2.85\times10^{-6}$ ph s^{-1} cm^{-2} with an exposure time of 10^6 s at 100 keV; see[8]) higher than the IC scattering of SMBH-ADAF photons, and is promising to detect the emissions to test the present model. However, INTEGRAL is not able to spatially resolve the region of the Galactic Center so that only upper limits are given by Malyshev et al. (2015). As to Fermi observations, the present model is not able to produce enough γ-ray emissions to explain the data. We agree that these γ-rays are from extended regions or other compact objects in the Galactic Center (Cafardo & Nemmen 2021).

3.3. mHz Gravitational Waves

If the $40M_\odot$ BH is orbiting around the central SMBH, Sgr A* will be an excellent target of LISA detection (Babak et al. 2017). From Equation (22), we find the strain amplitude $h_{\rm s}=1.4\times10^{-17}$, which is very strong for LISA. The decaying timescale of the orbits is $t_{\rm GW}\approx 32.9^{+28.4}_{-15.4}$ yr for $q_{\bar5}=1$, $M_6=4.3$, and $a_1=0.9$ in light of the current error bars of the orbital radius (A) from GRAVITY. More data are needed from GRAVITY to determine A better with higher statistics. The key test is from LISA to detect the strains and polarizations of the mHz GWs from the EMRI and its orbital decays. See some detailed calculations of mHz GWs from an EMRI, which can be found in Fang et al. (2019), Bondani et al. (2022), and Tahura et al. (2022). Considering the general relativistic effects, the Schartzshild procession of the sMBH is about $\Delta\phi\sim 6\pi R_{\rm g}/R_{\bullet}\approx 108^\circ\, r_{\rm l}^{-1}$ per period for a circular orbit. Therefore, it is feasible for GRVAVITY+/VLTI to measure the procession and decay of the orbit (through loci of the flare's location). Fully general relativistic treatments should be simultaneously done for both Schwartzschild procession and GWs. Sgr A* is an excellent laboratory for general relativity through GWs detected by LISA/Taiji/Tianqin, and orbits measured by GRAVITY+/VLTI.

4. Conclusions

We outline a model of the case of an sMBH as one satellite of the SMBH embedded in the ADAFs. The Bondi accretion onto the sMBH drives the formation of a cavity through outflows and leads to quenching the accretion. A cavity is expected to quasi-periodically appear in the SMBH-ADAF, and accumulated energies of sMBH outflows during its growth will make flares through viscous instability. Relativistic jets are developed by the Blandford–Znajek mechanism if the sMBH is maximally rotating, and will significantly emit nonthermal radiations spanning from radio to γ-rays. The nonthermal emissions from the relativistic jet follow the episodic cavities as quasi-periodic flickerings. Such an EMRI is an excellent laboratory for mHz GWs.

As a simple application of the present model, we explain the flares and quasi-periodic flickerings of Sgr A* within the framework of the present scenario. GRAVITY/VLTI maps of the locations of flares in Sgr A* consist of a ring, which supports the present model. The quasi-periodic flickerings are consistent with the flare's location, and flares take place driven by accumulations of about 10 flickerings. The satellite BH with $M_{\rm s}\approx 40M_\odot$ is favored from fitting the SED of Sgr A* spanning from radio to X-ray bands, where the relativistic jet is developed from the episodic sMBH-ADAF. The strain amplitudes of the mHz GWs are about 10^{-17}, and the sMBH will merge into the central SMBH in 30 yr. More precise measurements of the sMBH orbits are expected as well as mHz GW detections of LISA/Taiji/Tianqin to reveal the presence of the sMBH.

Though, we only provide formulations for an EMRI with a mass ratio of 10^{-5} around $10^6\,M_\odot$ SMBH, the present model is also applicable to $\gtrsim 10^6\,M_\odot$ system. Applications of the present scenario to other massive AGNs (e.g., Pyatunina et al. 2006) or 3C 390.3-like radio galaxies (Sergeev 2020) will be carried out.

[8] https://www.cosmos.esa.int/web/integral/instruments-ibis

For high-q systems, such as $q \sim 10^{-2}$, the properties of the system will be different from the present descriptions, showing much larger cavities than the low-q ones. In such a context, the EMRI system shows large amplitudes of flares, i.e., an upon-down mode of variabilities, and flickerings appear or disappear depending on the sMBH spins.

Finally, we would like to point out the possibility that multiple sMBHs may simultaneously coexist and randomly distribute inside the SMBH-ADAF. Since the properties of sMBH cavities are sensitive to the locations and masses, the flickerings and flares are superposed on each other. The quasi-periodicity of light curves arising from all of them may disappear but show random behaviors. In general, light curves of LLAGNs should be complicated if they contain multiple sMBHs.

Acknowledgments

The authors thank an anonymous referee for a helpful report. J.M.W. thanks F. Yuan and Z.-Q. Shen for useful discussions as to the physics of the Galactic Center. Helpful discussions are acknowledged with members from IHEP AGN Group. J.M.W. thanks the support by the National Key R&D Program of China through grants 2016YFA0400701 and 2020YFC2201400 by NSFC-11991050, -11991054, -11833008, -11690024, and by grant No. QYZDJ-SSW-SLH007 and No. XDB23010400. L.C.H. was supported by the NSFC (11721303, 11991052, 12233001), the National Key R&D Program of China (2022YFF0503401), and the China Manned Space Project (CMS-CSST-2021-A04, CMS-CSST-2021-A06). Y.F.Y. is supported by National Square Kilometre Array Program of China No. 2020SKA0120300 and National Natural Science Foundation of China (grant No. 11725312).

Appendix
Other Processes of Cavity Formation

In order to form a cavity, the sMBH-outflows should work to overcome possible barriers. First, the outflows work against the gravitational energy between the sMBH and the cavity gas. This means $\Delta E_1 = GM_s \Delta M_{cav}/R_{cav}$, where $\Delta M_{cav} = \frac{4\pi}{3} R_{cav}^3 n_e m_p$. We have the timescale of cavity formation

$$\Delta t_1 = 31.1\ \eta_{0.1}^{-1/3} \alpha_{0.1}^{-2/3} r_1^{7/6} q_{\bar{5}}^{1/3} \left(\frac{M_6}{4}\right) \mathrm{s}, \quad \text{(A1)}$$

where $\eta_{0.1} = \eta_{out}/0.1$. Second, the outflows should overcome the SMBH binding energy, and $\Delta E_2 = \Delta M_{cav}(GM_p/R_\bullet^2)R_{cav}$. The timescale is given by

$$\Delta t_2 = 31.9\ \eta_{0.1}^{1/3} \alpha_{0.1}^{-4/3} r_1^{11/6} q_{\bar{5}}^{2/3} \left(\frac{M_6}{4}\right) \mathrm{s}. \quad \text{(A2)}$$

The above estimations show that the outflows can easily make a cavity. Third, the outflows should work against the gas pressure of the SMBH-ADAF, that is $\Delta E_3 = \frac{4\pi}{3} R_{cav}^3 P_{gas}$ in the main text (e.g., McNamara & Nulsen 2007; Fabian 2012). Comparing the three cases, we find that the third case can make a much larger cavity than the other two.

ORCID iDs

Jian-Min Wang https://orcid.org/0000-0001-9449-9268
Jun-Rong Liu https://orcid.org/0000-0003-3086-7804
Yan-Rong Li https://orcid.org/0000-0001-5841-9179
Yu-Yang Songsheng https://orcid.org/0000-0003-4042-7191
Ye-Fei Yuan https://orcid.org/0000-0002-7330-4756
Luis C. Ho https://orcid.org/0000-0001-6947-5846

References

Abbott, R., Abbott, T. D., Abraham, S., et al. 2020, PhRvL, 125, 101102
Aimar, N., Dmytriiev, A., Vincent, F. H., et al. 2023, A&A, 672, A62
Armitage, P. J., & Natarajan, P. 1999, ApJL, 523, L7
Aschenbach, B., Grosso, N., Porquet, D., & Predehl, P. 2004, A&A, 417, 71
Babak, S., Gair, J., Sesana, A., et al. 2017, PhRvD, 95, 103012
Ball, D., Özel, F., Psaltis, D., & Chan, C.-K. 2016, ApJ, 826, 77
Barriére, N. M., Tomsick, J. A., Baganoff, F. K., et al. 2014, ApJ, 786, 46
Bartos, I., Kocsis, B., Haiman, Z., & Márka, S. 2017, ApJ, 835, 165
Bellovary, J. M., Low, M.-M.-M., McKernan, B., & Ford, K. E. S. 2016, ApJL, 819, L17
Blandford, R., & Begelman, M. L. 1999, MNRAS, 303, L1
Blandford, R., & Eichler, D. 1987, PhR, 154, 1
Blandford, R. D., & Znajek, R. L. 1977, MNRAS, 179, 433
Blumenthal, G. R., & Gould, R. J. 1970, RvMP, 42, 237
Bondani, S., Haardt, F., Sesana, A., et al. 2022, PhRvD, 106, 043015
Boyce, H., Haggard, D., Witzel, G., et al. 2022, ApJ, 931, 7
Cafardo, F., & Nemmen, R. 2021, ApJ, 918, 30
Cao, X. 2011, ApJ, 737, 74
Cao, X., & Rawlings, S. 2004, MNRAS, 349, 1419
Chan, C.-K., Liu, S.-M., Fryer, C.-L., et al. 2009, ApJ, 701, 521
Chen, L., & Zhang, B. 2021, ApJ, 906, 105
Chen, Y.-J., Bao, D.-W., Zhai, S., et al. 2023, MNRAS, 520, 1807
Cheng, K. S., & Wang, J.-M. 1999, ApJ, 521, 502
Chernyakova, M., Malyshev, D., Aharonian, F. A., et al. 2011, ApJ, 726, 60
Collin, S., & Zahn, J.-P. 1999, A&A, 344, 433
Collin, S., & Zahn, J.-P. 2008, A&A, 477, 419
Contopoulos, J., & Kazanas, D. 1995, ApJ, 441, 521
Dexter, J., Tchekhovskoy, A., Jiménez-Rosales, A, et al. 2020, MNRAS, 497, 4999
Do, T., Ghez, A. M., Morris, M. R., et al. 2009, ApJ, 691, 1021
Dodds-Eden, K., Porquet, D., Trap, G., et al. 2009, ApJ, 698, 676
Du, P., & Wang, J.-M. 2014, MNRAS, 438, 2828
Eckart, A., Baganoff, F. K., Schödel, R., et al. 2006, A&A, 450, 535
EHT Collaboration, Akiyama, K., et al. 2022, ApJL, 930, L12
Fabian, A. C. 2012, ARA&A, 50, 455
Fan, X., & Wu, Q. 2023, ApJ, 944, 159
Fang, Y., Chen, X., & Huang, Q.-G. 2019, ApJ, 887, 210
Fragione, G., & Loeb, A. 2022, ApJL, 932, L17
Frank, J., King, A., & Raine, D. J. 2002, Accretion Power in Astrophysics (3rd ed.; Cambridge: Cambridge Univ. Press)
Genzel, R., Eisenhauer, F., & Gillessen, S. 2010, RvMP, 82, 3121
Genzel, R., Schödel, R., Ott, T., et al. 2003, Natur, 425, 934
Georganopoulos, M., & Marscher, A. P. 1998, ApJ, 506, 621
Ghisellini, G., Maraschi, L., & Treves, A. 1985, A&A, 146, 204
Ghisellini, G., Padovani, P., Celotti, A., et al. 1993, ApJ, 407, 65
Ghosh, P., & Abramowicz, M. 1997, MNRAS, 292, 887
Goodman, J. 2003, MNRAS, 339, 937
Goodman, J., & Tan, J. C. 2004, ApJ, 608, 108
Graham, M., McKernan, B., Ford, K. E. S., et al. 2023, ApJ, 942, 99
Graham, M. J., Ford, K. E. S., McKernan, B., et al. 2020, PhRvL, 124, 251102
Gravity Collaboration 2022, A&A, 657, L12
Gravity Collaboration 2023a, A&A, 677, L10
Gravity Collaboration 2023b, A&A, 672, 63
Grishin, E., Bobrick, A., Hirai, R., et al. 2021, MNRAS, 507, 156
Hamann, F., & Ferland, G. 1999, ARA&A, 37, 487
Ho, L. C. 2002, ApJ, 564, 120
Hu, W.-R., & Wu, Y.-L. 2017, Natl. Sci. Rev., 4, 685
Igumenshchev, I. V., Illarionov, A. F., & Abramowicz, M. A. 1999, ApJL, 517, L551
Impellizzeri, C. M. V., Gallimore, J. F., Baum, S. A., et al. 2019, ApJL, 884, L28
Inoue, S., & Takahara, F. 1995, ApJ, 463, 555
Kolykhalov, P. I., & Sunyaev, R. A. 1980, SvAL, 6, 357
Leibowitz, E. 2021, ApJ, 915, 2
Li, Y.-R., Wang, J.-M., Ho, L. C., et al. 2016, ApJ, 822, 4
Li, Y.-R., Wang, J.-M., Zhang, Z.-X., et al. 2019, ApJS, 241, 33
Li, Y.-R., Yuan, Y.-F., Wang, J.-M., et al. 2009, ApJ, 699, 513
Lin, X., Li, Y.-P., & Yuan, F. 2023, MNRAS, 520, 1271
Lind, K. L., & Blanford, R. 1985, ApJ, 295, 358

Livio, M., Pringle, J., & King, A. 2003, ApJ, 593, 184
Luo, J., Chen, L.-S., Duan, H.-Z., et al. 2016, CQGra, 33, 035010
Macdonald, D., & Thorne, K. S. 1982, MNRAS, 198, 345
Mahadevan, R., Narayan, R., & Krolik, J. 2003, ApJ, 486, 268
Malyshev, D., Chernyakova, D., Neronov, A., et al. 2015, A&A, 582, 11
Manmoto, T. 2000, ApJ, 534, 734
Markoff, S., Falcke, H., Yuan, F., et al. 2001, A&A, 379, L13
McKernan, B., Ford, K., Lyra, W., et al. 2012, MNRAS, 425, 460
McNamara, B. R., & Nulsen, P. E. J. 2007, ARA&A, 45, 117
Mellah, I. E., Cerutti, B., & Crinquand, B. 2023, A&A, 677, 67
Mészáros, P. 2002, ARA&A, 40, 137
Michail, J. M., Yusef-Zadeh, F., Wardle, M., & Kunneriath, D. 2023, MNRAS, 520, 2644
Middelberg, E., Roy, A. L., Nagar, N. M., et al. 2004, A&A, 417, 925
Nagao, T., Maiolino, R., & Marconi, A. 2006, A&A, 447, 863
Naoz, S., Will, C. M., Ramirez-Ruiz, E., et al. 2020, ApJL, 888, L8
Narayan, R., & Yi, I. 1994, ApJL, 428, L13
Narayan, R., & Yi, I. 1995, ApJ, 452, 710
Narayan, R., Yi, I., Mahadevan, R., et al. 1995, Natur, 374, 623
Oka, K., & Manmoto, T. 2003, MNRAS, 340, 543
Okuda, T., Singh, C. B., & Ramiz, A. 2023, MNRAS, 522, 1814
Paczyński, B. 1978, AcA, 28, 91
Peters, P. C. 1964, PhRv, 136, 1224
Ponti, G., George, E., Scaringi, S., et al. 2017, MNRAS, 468, 2447
Pyatunina, T. B., Kudryavtseva, N. A., Gabuzda, D. C., et al. 2006, MNRAS, 373, 1470
Rauch, C., Ros, E., Krichbaum, T. P., et al. 2016, A&A, 587, 37
Rees, M. J. 1984, ARA&A, 22, 471
Rees, M. J., Begelman, M. C., Blandford, R. D., et al. 1982, Natur, 295, 17
Samsing, J., Bartos, I., D'Orazio, D. J., et al. 2022, Natur, 603, 237
Secunda, A., Bellovary, J., Low, M. M. M., et al. 2019, ApJ, 878, 85
Sergeev, S. G. 2020, MNRAS, 495, 971
Shakura, N. I., & Sunyaev, R. A. 1973, A&A, 24, 337
Shin, J., Woo, J.-H., Nagao, T., et al. 2013, ApJ, 763, 58
Shlosman, I., & Begelman, M. C. 1989, ApJ, 341, 685
Sikora, M., Begelman, M., & Rees, M. J. 1994, ApJ, 421, 153
Sikora, M., Stawarz, Ł., & Lasota, J.-P. 2007, ApJ, 658, 815
Stone, N. C., Metzger, B. D., & Haiman, Z. 2017, MNRAS, 464, 946
Tadhunter, C. 2016, A&ARv, 24, 10
Tagawa, H., Haiman, Z., & Kocsis, B. 2020, ApJ, 898, 25
Tahura, S., Pan, Z., & Yang, H. 2022, PhRvD, 105, 123018
Thompson, T. A., Quataert, E., & Murray, N. 2005, ApJ, 630, 167
Volonteri, M., Sikora, M., Lasota, J.-P., et al. 2013, ApJ, 775, 94
von Fellenberg, S. D., Gillessen, S., Stadler, J., et al. 2022, ApJL, 932, L6
von Fellenberg, S. D., Witzel, G., Bauböck, M., et al. 2023, A&A, 669, L17
Wang, J.-M., Cheng, C., & Li, Y.-R. 2012a, ApJ, 748, 147
Wang, J.-M., Du, P., Baldwin, J. A., et al. 2012b, ApJ, 746, 137
Wang, J.-M., Ge, J.-Q., Hu, C., et al. 2011, ApJ, 739, 3
Wang, J.-M., Hu, C., Li, Y.-R., et al. 2009, ApJL, 697, L141
Wang, J.-M., Liu, J.-R., Ho, L. C., et al. 2021a, ApJL, 911, L14
Wang, J.-M., Liu, J.-R., Ho, L. C., et al. 2021b, ApJL, 916, L17
Wang, J.-M., Yan, C.-S., Gao, H.-Q., et al. 2010, ApJL, 719, L148
Wang, J.-M., Zhai, S., Li, Y.-R., et al. 2023, ApJ, 954, 84
Wang, Q. D., Nowak, M. A., Markoff, S. B., et al. 2013, Sci, 341, 981
Wang, X., & Loeb, A. 2014, MNRAS, 441, 809
Warner, C., Hamann, F., & Dietrich, M. 2003, ApJ, 596, 72
Will, C. M., Noaz, S., Hees, A., et al. 2023, arXiv:2307.16646
Witzel, G., Martinez, G., Willner, S. P., et al. 2021, ApJ, 917, 73
Woosley, S. E., Heger, A., & Weaver, T. A. 2002, RvMP, 74, 1015
Xu, Y., Narayan, R., Quataert, E., et al. 2006, ApJ, 640, 319
Yang, Y., Bartos, I., Gayathri, V., et al. 2019, PhRvL, 123, 181101
Yuan, F., Quataert, E., & Narayan, R. 2003, ApJ, 598, 301
Yusef-Zadeh, F., Bushouse, H., Wardle, M., et al. 2009, ApJ, 706, 348
Zhang, S.-R., Luo, Y., Wu, X.-J., et al. 2023, MNRAS, 524, 940
Zhu, J.-P., Yang, Y.-P., Zhang, B., et al. 2021a, ApJL, 914, L19
Zhu, J.-P., Zhang, B., Yu, Y.-W., et al. 2021b, ApJL, 906, L11